HHS Public Access

Author manuscript

Drug Chem Toxicol. Author manuscript; available in PMC 2023 March 01.

Published in final edited form as:

Drug Chem Toxicol. 2022 March ; 45(2): 767–774. doi:10.1080/01480545.2020.1774774.

Real-time monitoring of cellular oxidative stress during aerosol sampling: a proof of concept study

Lynn E. Secondo[a,b], **Vitaliy Avrutin**[c], **Umit Ozgur**[c], **Erdem Topsakal**[c], **Nastassja A. Lewinski**[a]

[a]Department of Chemical and Life Science Engineering, Virginia Commonwealth University, Richmond, VA, USA

[b]Department of Electrical and Computer Engineering, Virginia Commonwealth University, Richmond, VA, USA

[c]Environmental and Occupational Health Sciences Institute, Rutgers University, Piscataway, NJ, USA

Abstract

The Portable *In Vitro* Exposure Cassette (PIVEC) was developed for on-site air quality testing using lung cells. Here, we describe the incorporation of a sensor within the PIVEC for real time monitoring of cellular oxidative stress during exposure to contaminated air. An electrochemical, enzymatic biosensor based on cytochrome c (cyt c) was selected to measure reactive oxygen species (ROS), including hydrogen peroxide and super oxides, due to the stability of signal over time. Human A549 lung cells were grown at the air–liquid interface and exposed within the PIVEC to dry 40 nm copper nanoparticle aerosols for 10 minutes. The generation of ROS compounds was measured during exposure and post-exposure for one hour using the biosensor and compared to intracellular ROS determined using the 2′,7′-dichlorodihydrofluoroscein diacetate (DCFH-DA) assay. A similar increase in oxidative stress upon aerosol exposure was measured using both the cyt c biosensor and DCFH-DA assay. The incorporation of a biosensor within the PIVEC is a unique, first-of-its-kind system designed to monitor the real-time effect of aerosols.

Keywords

Biosensor; copper particles; inhalation; nanoparticle; *in vitro*

Introduction

Real-time monitoring allows for rapid determination of changes in the environment. During air quality monitoring, aerosol concentration is measured based on particle number using particle counters (Matson et al. 2004, Mills et al. 2013) or mass by gravimetric analysis.

CONTACT Nastassja A. Lewinski, nalewinski@vcu.edu, Department of Chemical and Life Science Engineering, Virginia Commonwealth University, Richmond, VA, USA.

Disclosure statement

The authors report no conflict of interest.

Volatile organic compound (VOC) and gas sensors are available to monitor various gaseous compounds (Vilcekova et al. 2013, Gerhardt et al. 2014). While these techniques provide data related to exposure, they do not directly inform on the potential hazard. Hazard relationships can be determined by integrating real-time monitoring of biological endpoints with cellular exposure, allowing information relating to the particle-cell interactions to be gained.

Biological endpoints, such as oxidative stress, inflammation, and cytotoxicity are traditionally measured using dye-based assays. Oxidative stress results from an increase in reactive oxygen species (ROS) generation, a decrease in antioxidant capacity, or a combination of these processes. ROS species, which include superoxide ($O_2^{\cdot-}$) radicals, hydroxyl ($OH^{\cdot}$) radicals, and hydrogen peroxide (H_2O_2) (Halliwell and Whiteman 2004), are utilized within a cell for signaling purposes (Murphy 2009, Santschi et al. 2017). As the balance between oxidants and antioxidants changes, the cell cycle is disrupted through DNA and lipid oxidation (Davies 1999, Chiu and Dawes 2012, Carrasco-Torres et al. 2017), and cell damage may occur due to oxidation by free radicals. Oxidative stress and inflammation are closely linked endpoints within the biological response. There is often a cyclic relationship between increased oxidative stress and increased inflammation which has been implicated in adverse outcome pathways (Savolainen et al. 2013, Wittekindt et al. 2014, Vietti et al. 2016, Santschi et al. 2017) leading to cancer, fibrosis, or pulmonary disorders. Changes in ROS concentration has been used as a biomarker for hazard assessment (Oberdörster et al. 2005, Park et al. 2008, Bérubé et al. 2009, Lewinski et al. 2018). Oberdörster et al. (2005) describe oxidative stress as a dominant mechanism for cell damage that is an endpoint to detect the effects of nanoparticle exposures both *in vitro* and *in vivo.* Particularly, oxidative stress is helpful in determining potential inflammation in the epithelium, endothelium, macrophages, and fibroblasts within the lung.

Biosensors for oxidative stress measurement focus on the detection of specific ROS, with current systems designed to monitor H_2O_2 and superoxide (Prieto-Simón et al. 2008, Calas-Blanchard et al. 2014). Three main types of enzymatic sensors have been developed for oxidative measurements using cytochrome c (cyt c), superoxide dismutase (SOD), and horseradish peroxidase (HRP). Focusing on cyt c, cyt c is known to measure both H_2O_2 and superoxide radicals (Banan Sadeghian et al. 2017). Cyt c based sensors have been used *in vitro* and have been shown to have relatively fast electron shuttling, decreasing the response time (Calas-Blanchard et al. 2014, Eguílaz et al. 2016, Liu et al. 2016, Sadeghian et al. 2016, Thirumalai et al. 2017). The ability for cyt c to measure both H_2O_2 and superoxide radicals through direct electron transfer allows the opportunity to measure at potentials that minimize possible anodic and cathodic interferences (Chen et al. 2012). Common methods for applying the enzyme to the working electrode include drop casting (Li et al. 2010, Rahimi et al. 2011, Ganesana et al. 2012, Eguílaz et al. 2016, Sadeghian et al. 2016, Banan Sadeghian et al. 2017) and covalent bonding through immersion in a cyt c solution (Bowden et al. 1984, Cai et al. 1995, Tammeveski et al. 1998, Chen et al. 2008, Luo et al. 2009, Zhu et al. 2009, Zhou et al. 2014, Thirumalai et al. 2017). Cyt c has been shown to have high selectivity against many biologically active compounds including dopamine, ascorbic acid, uric acid, oxygen, and reactive nitrate species (Luo et al. 2009, Rui et al. 2010). In addition, cyt c based sensors have been used *in vitro* for the measurements of ROS in milk and mouthwash

(Eguílaz et al. 2016), bacterial cultures, (Liu et al. 2016), cancerous cell cultures (Luo et al. 2009, Rui et al. 2010, Zhou et al. 2014), and *ex vivo* mouse brain slices (Ganesana et al. 2012). Eguílaz et al. (2016) made a biosensor by depositing a multiwalled carbon nanotube (MWCNT)-cyt c solution on a glassy carbon electrode and characterized the sensor in phosphate-buffered saline (PBS) with H_2O_2 concentrations up to 300 μM. The co-deposition of MWCNT and enzyme provided a highly reproducible and reusable electrode. The sensor was then used to determine the H_2O_2 content in mouthwash and spiked low-fat milk samples with a less than 2% deviation from standard values. Liu et al. (2016) monitored the oxidative stress induced by antibiotics in a bacterial culture using a cyt c sensor. The sensor was based on a gold wire working electrode, decorated with gold nanoparticles to which thiols were immobilized to enhance the covalent bonding of the enzyme. Using amperometry, the sensor was characterized in cell culture media at a theoretical concentration up to 1 μM superoxide generated by xanthine oxidase. The oxidative stress generated by antibiotic interaction with the bacteria was not pronounced enough to be the sole contribution to bacterial death. The H_2O_2 release of Hep G2 cells, a human hepatocellular carcinoma cell line, was measured by Rui et al. (2010), Luo et al. (2009), and Zhou et al. (2014). Sensors were fabricated through the covalent bonding of cyt c onto ZnO nanosheets (Rui et al. 2010) or TiO_2 nanoparticles (Luo et al. 2009) or the cross-linking of the enzyme within a hydrogel matrix (Zhou et al. 2014). Characterization was performed in PBS with H_2O_2 concentrations up to 1 mM. Similar results were observed between each experimental set up, reducing current with the addition of phorbol 12-myristate 13-acetate (PMA) and increasing with the addition of catalase to the cells (Luo et al. 2009, Rui et al. 2010, Zhou et al. 2014). Ganesana et al. (2012) monitored the real-time release of superoxide in CD-1 mouse brain slices using cyt c modified gold electrodes during normal physiological conditions, ischemia, and exposure to ceria nanoparticles. High temporal resolution, sensitivity, and selectivity were observed in the normal conditions. Superoxide levels quickly increased during ischemia which were then reduced over 8% through the addition of ceria nanoparticles (Ganesana et al. 2012). These studies provide a good basis for the design and testing of a cyt c based sensor. The sensor presented in this work provides a similar linear response and sensitivity to cancer cells; however, often the signal is higher, allowing for additional discrimination of small changes in concentration.

In both *in vitro* and *in vivo* models, exposure to aerosols containing copper nanoparticles have been reported to induce oxidative stress, inflammation, and cytotoxicity. Studies performed at the ALI using A549 cells report increases in copper toxicity and ROS observed using 9.2 nm particles at 83 ng/well or 12 nm particles at 4.6 μg deposited dose. (Kim et al. 2013, Jing et al. 2015). Lethal concentration 50 (LC50) values in A549 cells at 24 hours post exposure to CuO nanoparticles were determined to be <25 $\mu g/cm^2$ (Aufderheide et al. 2013) and 2 $\mu g/cm^2$ (Frijns et al. 2017). *In vivo* toxicity (Cho et al. 2012) and increases in ROS generation (Rani et al. 2013, Lai et al. 2018) are also observed. Inhalation studies were performed at acute and sub-acute levels, producing deposited doses of 10.8–63.6 μg of 9.2 nm copper nanoparticles (Pettibone et al. 2008) and 0.23 mg of 25 nm copper oxide particles (Gosens et al. 2016). Sub-acute inhalation of copper based nanoparticles induced increases in macrophage, neutrophil, and lymphocyte response (Pettibone et al. 2008, Kim et al. 2011, Gosens et al. 2016). The lactate dehydrogenase (LDH) response determined by Kim et al.

(2011) was similar for inhaled particles and instillation, where there was an increase of approximately three times of deposited dose. Cytokine increases of IL-6, GM-CSF, and TNF-a, representing inflammation, were also observed in sub-acute dosages (Pettibone et al. 2008, Kim et al. 2011). As copper ions are considered toxic, the dissolution of these particles was determined in Gamble's solution, a solution that mimics airway surface fluid. Within one hour of exposure of copper-based particles, there was an increase of copper ions of approximately 2% (Pettibone et al. 2008, Gosens et al. 2016). More acidic solutions, pH 4.5–5.0, completely dissolved the nanoparticles within 24 h of exposure (Pettibone et al. 2008, Gosens et al. 2016). With strong toxicity observed at 24 hours post exposure, understanding the rate of change during the exposure process could provide new insights.

There are few air-liquid interface (ALI) exposure systems that utilize real-time biological measurements. By adding an ROS biosensor to the Portable *In Vitro* Exposure Cassette (PIVEC, Secondo et al. 2019) users can explore how exposure to different aerosols and gases can disturb redox homeostasis in lung cells. A cyt c functionalized biosensor was incorporated to determine the change in ROS concentration during exposure. The sensor was calibrated with H_2O_2, tested in physiological buffers for linearity of response, and compared to intracellular ROS measured using the DCFH-DA assay post-exposure to 40 nm copper nanoparticles.

Materials and methods

The design of an enzymatic biosensor was focused on the functionalized working electrode and the ability to transfer ions from the reaction substrate to the electrode for measurement. The working electrode was designed using metal oxide nanostructures, providing additional surface area for enzyme deposition and an opportunity for electron shuttling from the enzyme to the electrode (Scognamiglio 2013). Once functionalized, the electrochemical response of the working electrode was measured as a function of electrolyte composition, as response may vary with electrolyte composition, pH, and temperature (Cai et al. 1995, Allen et al. 1997, Avila et al. 2000, Gomez-Mingot et al. 2014). Materials for sensor fabrication included zinc nitrate hydrate, platinum and silver electroplating solutions, medical grade silicone, cyt c from equine heart, and a Nafion solution. For cell culture, materials from Gibco include Dulbecco's modified Eagle medium, fetal bovine serum, PBS, and Hank's buffered salt solution (HBSS). Exposure and cellular response was performed using copper nanoparticles from U.S. Research Nanomaterials, Inc. (Houston, TX), and the DCFH-DA assay from Sigma-Aldrich (St. Louis, MO).

Sensor fabrication and functionalization

A coplanar, tri-electrode sensor was produced using a ZnO nanostructured working electrode and platinum/gold and anodized silver on sapphire as counter electrode and reference electrode, respectively. The working electrode was fabricated using conventional photolithography followed by metal evaporation and liftoff to produce a patterned gold/titanium electrode on sapphire on which nanostructured ZnO rods were grown. An advantage of ZnO is that it can be easily produced in the form of various nanostructures (e.g., nanowires, nanobelts, and nanotubes) with high surface-to-volume ratio that

substantially enhance sensor sensitivity (Izyumskaya et al. 2017). In this work, ZnO nanorods were grown electrochemically in 0.025 M zinc nitrate hydrate ($Zn(NO_3)_2 \cdot 6H_2O$) aqueous solution at 90 °C. The electrodeposition was performed using square pulses, 0.25 Hz frequency, 50% duty circle with varying peak currents. The morphology of nanorods grown by this method was studied as a function of the process current using scanning electron microscopy (SEM, Hitachi SU-7, Tokyo, Japan). To ensure the highest enzyme load, nanorods with the highest aspect ratio of 13 (with diameter and length of approximately 100–150 nm and 2 μm, respectively), fabricated at a current density of 0.625 mA/cm^2, were used to produce the working electrode. Figure 1(a) provides a scanning electron microscope (SEM, Hitachi SU-7, Tokyo, Japan) image of the nanorods at 17–20 $rods/cm^2$. This provides approximately 13.5 times more surface area than a flat film.

Prior to sensor functionalization, 32 gauge wire pieces are prepared and soldered to each electrode. The indium solder is covered using a medical grade silicone (Silastic MDX 4-4210, Dow Corning, Midland, MI), providing a barrier to enhance the biocompatibility and mechanical stability of the electrical connection. To functionalize the working electrode for H_2O_2 detection, 20 μL of a 0.67 mM (8 mg/1 mL) solution in 0.01 M PBS (pH 7.4) of cyt c (from equine heart, Sigma-Aldrich, St. Louis, MO) was drop cast onto the ZnO nanowires and allowed to dry. Cyt c has been shown to have a high affinity for ZnO, binding over 90% of free proteins to the surface maintaining structure with little degradation (Šimšíková and Antalík 2013). Unbound and loosely adsorbed cyt c was then removed by rinsing the functionalized electrode with approximately 1 mL of 0.01 M PBS. Once dried, 20 μL of a 5wt% Nafion solution (Sigma-Aldrich, St. Louis, MO) was spin coated to form a 40 nm thick membrane. The platinum and silver thin films were grown on sapphire substrates by electrodeposition using commercially available solutions (Pt: EPi 50/50 Ready to Plate, Ag: Technic Elevate). Anodization of the silver thin film was performed in a solution of 0.01 M PBS at 1.5 V for three minutes to form a layer of silver chloride. To form a single, coplanar tri-electrode sensor, the functionalized working electrode, platinum thin film, and anodized silver thin film are then individually affixed using a layer of medical grade silicone to a single sapphire wafer. The sapphire wafer is cut to a width of approximately 12 mm to minimize the possibility for variation in sensor alignment. The design of the sensor is shown in Figure 1.

Electrochemical testing of cytochrome c sensor

A 100 μM stock solution of H_2O_2 was used to simulate ROS increases in concentration and stimulate electrochemical reactions. All solutions were warmed to 37 °C prior to electrochemical testing and maintained at 37 ±1 °C during testing through the use of a resistive heater and direct current (DC) power supply set to 5 V providing roughly 0.55 A. Baseline measurements were performed in 20 mL of Hank's Balanced Salt Solution (HBSS, Gibco, Waltham, MA) or PBS (Gibco, Waltham, MA) to which the stock solution of H_2O_2 is added. Cyclic voltammetry (CV) measurements were performed in HBSS or PBS buffer solution at 37 °C. CV parameters were adjusted to sweep from −1 V to 1.5 V versus Ag/AgCl at 50 mV/s and the concentration of H_2O_2 was increased from 0.1 μM to 10 μM, see Table S1 for full CV testing scheme. Chronoamperometry was performed at 1 V versus Ag/AgCl and the H_2O_2 concentration adjusted every 180 s over the same concentration

range, see Table S2 for full amperometric testing scheme. The solution was continuously stirred using a magnetic stir bar during chronoamperometric measurements. Specific added volume values of the H_2O_2 stock solution are described in the Supplemental information testing scheme tables. All electrochemical measurements were performed using a VersaStat 3 potentiostat galvanostat (Princeton Applied Research, Oak Ridge, TN).

Incorporation of sensor within PIVEC

The PIVEC is a unique system that allows for the exposure of cells to aerosols or gases outside of the laboratory environment (Secondo et al. 2019). A cassette adapter is used to sustain *in vitro* conditions during the exposure period. The cell model used for inhalation effects was the human alveolar epithelial adenocarcinomic A549 cell line (Lieber et al. 1976). The A549 cell line, a type II alveolar epithelial cell, has been used by several groups to test toxicity and for characterization of *in vitro* exposure systems (de Bruijne et al. 2009, Lenz et al. 2009, Asimakopoulou et al. 2013, Aufderheide et al. 2003, 2013, Elihn et al. 2013, Fröhlich et al. 2013). Cells were cultured in culture media consisting of Dulbecco's modified Eagle medium (Gibco, Waltham, MA) with 1% penicillin–streptomycin and 10% fetal bovine serum (Gibco, Waltham, MA). After reaching confluency, cells were trypsinized, pelleted, counted using a hemocytometer, and suspended to a concentration of 140 000 cells/mL using culture media. From this cell suspension, 35 000 cells were added to the apical side of a 24-well cell culture insert (Corning Costar, Collagen coated, 6.5 mm diameter, 0.4μm pore size). After seven days with media exchange every two days, the apical media was removed and cells were allowed to equilibrate at the ALI for 24 h prior to exposure. This cell culture protocol has been shown to produce a cellular monolayer expressing tight junction proteins and a surfactant layer, similar to *in vivo* models (Blank et al. 2006). However, A549 is a cancerous cell line, which may influence the cellular sensitivity of response.

To induce a biological response, copper nanoparticles (U.S. Research Nanomaterials, Inc., Houston, TX) of 40 nm diameter were used. A custom, dry aerosol dispersal system, based on the design reported by Tiwari et al. (2013) was connected to compressed air to generate a particle dispersion (Secondo et al. 2019). The aerosol then traveled to the PIVEC (Secondo et al. 2019) as it was pulled through the system by a vacuum pump set at 500 mL/min. The full experimental set-up is described in Figure S1 of the supplemental information. Cells were exposed for a total of 10 min and returned to the incubator for post-exposure analysis using a dye-based assay or remained in the PIVEC to be monitored via the biosensor.

Generation of ROS was determined using 2′,7′-dichlorodihydrofluoroscein diacetate (DCFH-DA, Sigma-Aldrich, St. Louis, MO) indicator dye (Carter et al. 1994). Although DCFH-DA is non-fluorescent, after entering the cell, the diacetate group is enzymatically cleaved from the compound, producing dichlorofluorescein that is fluorescently detectable once oxidized through intracellular ROS. Briefly, cells at the ALI were washed with PBS (Gibco, Waltham, MA) and 0.5 mL of 10 μM DCFH-DA in HBSS (Gibco, Waltham, MA) was placed basolaterally and kept for an hour within the incubator to allow the cells to take up the dye. After incubation, the diluted DCFH-DA solution was removed and replaced with 0.5 mL warmed HBSS and an initial reading taken. Fluorescence measurements of

the oxidized DCF were taken using a plate reader (Cytation 3, BioTek, Winooski, VT) with excitation/emission wavelengths of 485/530 nm. After exposure, measurements were continued every minute for one hour. Results are reported as fluorescence increase relative to the initial reading of each sample.

The coplanar electrochemical biosensor was positioned on the basolateral side of the ALI cells to measure the diffused H_2O_2 generated by the cells. The cell culture insert was loaded into the PIVEC with 2 mL of HBSS within the well containing the sensor. The PIVEC set-up was completed following the protocol described by Secondo et al. (2019) and was connected to the dry air dispersal system and vacuum pump. Baseline electrochemical measurements were performed for five minutes prior to exposure using amperometry at 1 V versus Ag/AgCl.

Cells were exposed to copper nanoparticles while continuing to monitor oxidative stress using the amperometric biosensor. Briefly, copper nanoparticles were loaded into the dry aerosol dispersal system and aerosolized using a clean air cylinder following Secondo et al. (2019). After complete aerosolization, the inlet air from the cylinder was turned off and the vacuum pump continued to run. The deposited dose of copper was 0.44 mg during 10 minutes of exposure at an aerosol flow rate of 0.5 LPM. The cells and sensor remained inside the PIVEC post-exposure, maintained at 37 °C. The generation of ROS was monitored through amperometric measurements every half second using the biosensor. This was continued for 1 h post-exposure.

Each experiment was run in triplicate unless otherwise noted. The average and standard deviation of each set was taken. With small data sets, analysis of variance (ANOVA) single factor analysis was performed to determine significance between data sets. Where applicable, Student's *t*-tests were performed to determine statistically significant data points. Data are reported as the average ± standard deviation.

Results

The sensor was functionalized with cyt c deposited on ZnO nanorods for the electrochemical detection of ROS generation. Calibration was performed with different H_2O_2 concentrations in buffer solutions for quantification of sensor response during short term cellular exposures. Finally, the sensor response was compared post-exposure to the DCFH-DA assay.

Sensor fabrication

The base working electrode was 50 nm of Au on 20 nm titanium deposited on a sapphire substrate. The nanorods grown in this method were rod-like with a hexagonal cross section, aligned perpendicularly to the substrate. The diameter was controlled through the peak current density measured with SEM. Nanorods used for the functionalization were grown at 0.625 mA/cm^2 to produce average diameter of approximately 100–150 nm and a length of 2 μm. The deposition of cyt c on the ZnO nanorods was determined using three cycles varying scan rates (ν, 10 mV/s, 20 mV/s, 50 mV/s, 100 mV/s, 200 mV/s, and 500 mV/s) during the CV. Following an ideal Nernstian reaction under Langmuir isotherm conditions, the peak current observed is proportional to the scan rate applied using Equation (1). In this

equation, the number of electrons transferred, *n*, active area of 0.3 cm^2, A, Faraday constant, F, and gas constant, R, are used to determine the molar concentration of enzyme, Γ. A low concentration of 5 $nmol/cm^2$ was determined to be immobilized on the sensor.

$$i_p = \frac{n^2F^2}{4RT}Av\Gamma \quad (1)$$

Electrochemical characterization

The sensor was tested using CV to determine the ability to measure H_2O_2 and the ideal potential for amperometric testing. The sensor was tested in solutions of 0.01 M PBS, 1 M PBS, and 1 M HBSS. Calibration curves were determined at 1 V versus Ag/AgCl for both buffers. At all tested concentrations of PBS, no reaction peaks were observed, as shown in Figure S2 of the supplemental information. Additionally, little linearity was observed over the H_2O_2 concentration range of interest. When the sensor was tested in HBSS, defined redox peaks were observed near 1 V and 0.3 V (Figure 2), which is consistent with literature (Rodkey and Ball 1950, Gopal et al. 1988). Peak oxidative current at each concentration was used to determine a calibration curve. Sensor response over the desired H_2O_2 concentration range at 1 V includes a linear region from 0.01 μM to 7.5 μM H_2O_2 (Figure 3). The sensor response measured from this experiment was 248.48 μA/μM/cm^2 in HBSS.

Measurements can be affected by the ionic strength of the electrolyte, observed through the response in PBS. A 100× increase in ionic strength (*I*) was observed as a similarly proportional increase in current. The ionic strength of 1 M PBS and HBSS are very similar, $I_{PBS,\ 1\ M}$ = 152 mM and I_{HBSS} = 155 mM. Additional ions within the electrolyte may affect the ability to shuttle ions as there is more affinity to the solution than at low ionic concentrations. This is consistent with the findings of Avila et al. (2000) solutions of low ionic strength provided near independence of electron transfer. The Nafion membrane is cation permeable and diffusion relates to the cation charge and concentration of solution, therefore as HBSS has calcium and magnesium ions in solution, the sensor response is reduced compared to 1 M PBS, at 1 V and 0.1 μM H_2O_2 the currents are 74 μA and 1095 μA, respectively. Temperature, electrolytic compounds, and pH have also been shown to affect sensor response (Cai et al. 1995, Allen et al. 1997, Avila et al. 2000).

Real-time monitoring with the PIVEC

The sensor was calibrated prior to exposure, observed in Figure 3, to determine the H_2O_2 concentration during exposure. The H_2O_2 concentration was then normalized to the initial, baseline concentration and reported as the relative accumulation. The start of the exposure can be observed where the concentration spikes near 30 seconds (Figure 4). The real-time concentration of H_2O_2 was observed within two minutes of exposure.

Intracellular generation of ROS was measured using the DCFH-DA assay. There was a significant increase in fluorescence within one hour of exposure, observed in Figure 5. The extracellular ROS generation was monitored using the cyt c sensor. Comparing these techniques, increases in ROS within and outside of the cell membrane was observed after

30 min post-exposure. Accumulation of ROS measured using the biosensor is approximately equivalent to 1 μM of H_2O_2 compared to the intracellular ROS generation, approximately 80 μM H_2O_2.

Discussion

A biosensor was functionalized with cyt c for the electrochemical detection of ROS generation induced by the exposure of lung cells to an aerosol of copper nanoparticles. The increase in ROS was observed in real time using the biosensor and post exposure through the conventional DCFH-DA assay.

ROS generation was measured using two techniques. Intracellular measurement of ROS is performed through the DCFH-DA assay. The specificity of this assay is debated in literature (Lebel et al. 1992, Myhre et al. 2003, Kalyanaraman et al. 2012). Generation of ROS within the cell post-exposure can occur through particle or cell induced pathways. As the particle material used is copper, a transition metal, the potential for the cell to utilize Fenton-like and Haber-Weiss reactions (Haber and Weiss 1932) increases. Davies (1999) reported on varying levels of equivalent H_2O_2 and the cellular effects of the oxidative stress. Within the cell, the production of high levels of ROS has been shown to lead to cellular growth arrest at the equivalent of 120–150 μM H_2O_2, apoptosis at 0.5–1 mM H_2O_2 equivalent, or necrosis at levels 5–10 mM or higher equivalent H_2O_2 (Davies 1999). Using the cyt c functionalized sensor, the generation of extracellular ROS and leakage of ROS through the cellular membrane is observed near 1 μM H_2O_2 equivalent. Cyt c is nonselective toward H_2O_2 and superoxide ions and reflects the interaction with each species. Hydrogen peroxide can freely diffuse through the cell membrane; however, superoxide must be shuttled through anion transport mechanisms (Finkel 2003, Fisher 2009). This could account for the increase in ROS observed extracellularly. The intracellular measurement of ROS was approximately 80 μM H_2O_2 equivalent, suggesting that the expected toxic response to Cu NPs takes longer than one hour post exposure to observe even for a deposited dose of 0.44 mg.

Comparing the measurement techniques, increases in ROS are observed within the cell and in the basolateral fluid. There is a delay in the response for the sensor (Figure 5), likely due to the time for ROS to diffuse out of the cell before reaching the sensor. However, once the sensor signal begins to increase, the rate of response is faster than that measured by DCFH-DA. It is possible that initially highly reactive radical species are observed followed by the slower decomposition of H_2O_2. As expected due to measurement position, the equivalent H_2O_2 concentration measured extracellularly using the biosensor was significantly lower (1 μM) than the intracellular ROS measured using the DCFH-DA assay (80 μM). Effects of the method of exposure were observed within the sensor response. There is a sharp increase in current at the time of initial exposure as the air flow to aerosolize the nanopowder increases stresses upon the cell. This response could be mitigated through the reduction in flow rate necessary to aerosolize the nanopowder. However, as the exposure duration lengthens, the vehicle becomes more likely to induce higher stresses on the culture. Therefore, low flow rates and characterization of the biological response to the vehicle are keys.

While enzymatic biosensors are a promising method for real-time monitoring, limitations occur due to the enzyme selectivity and results can become convoluted. The enzymatic activity decreases over time due to instability, increasing the error and usefulness of the sensor. Throughout literature, the stability of cyt c based sensors was measured typically at one week to one month depending on storage conditions and use (Zhu et al. 2009, Thirumalai et al. 2017). The longest lasting sensor observed was for 180 days; however, it was stored the majority of the time (Rahimi et al. 2011). Due to operational nature, stability under continuous operation needs to be investigated. The use of a cyt c sensor allows for monitoring multiple ROS but does not allow for the specific determination of individual ROS to investigate response pathways. By utilizing sensors functionalized with other enzymes, SOD or HRP, the specific influence of individual ROS compounds can be determined.

The inclusion of a biosensor within an ALI exposure system allows for real-time monitoring during exposure, providing additional information that may be used to determine mechanisms of interactions between aerosols and cells and informing risk assessment. Advantages of using real-time monitoring include the ability to observe the exposure and potential effects of the exposure process and duration on the generation of ROS. As observed in Figure 4, the exposure can be observed as a spike in current.

This is one of the first studies to present a comparison of intracellular and extracellular ROS monitoring. The incorporation of a cyt c functionalized sensor allows for the real-time monitoring of oxidative stress generation within the PIVEC. The extracellular ROS observed using the biosensor was less than the intracellular generation, likely due to the differences in transport mechanisms. By changing the enzyme immobilized on the sensor, alternative biological endpoints can be monitored during exposure. This process will allow for insight to the cellular response to particle interactions and pathways of toxicity.

Supplementary Material

Refer to Web version on PubMed Central for supplementary material.

Acknowledgements

The authors acknowledge the Virginia Microelectronics Center for assistance in the fabrication of the biosensor. The author thank Kai Ding for their work in the fabrication process of the sensor including metal deposition and nanostructure growth and Shanzé Eshai and Jessi Shaffer for their work in the functionalization process of the sensor.

Funding

This work was supported by startup funds provided to Dr. Lewinski by the College of Engineering at Virginia Commonwealth University. Additionally, LES would like to acknowledge the NIEHS Training Grant [1T32ES019854, PIs: C. Weisel (Contact), G. Mainelis].

References

Allen H, et al. , 1997. The transient nature of the diffusion controlled component of the electrochemistry of cytochrome c at “bare” gold electrodes: an explanation based on a self-blocking mechanism. Journal of Electroanalytical Chemistry, 436 (1–2), 17–25.

Asimakopoulou A, et al. , 2013. Development of a dose-controlled multiculture cell exposure chamber for efficient delivery of airborne and engineered nanoparticles. Journal of Physics: Conference Series, 429, 12023–12010.

Aufderheide M, et al. , 2013. The CULTEX RFS: a comprehensive technical approach for the in vitro exposure of airway epithelial cells to the particulate matter at the air-liquid interface. BioMed Research International, 2013, 734137–734115. [PubMed: 23509768]

Aufderheide M, Knebel JW, and Ritter D, 2003. An improved in vitro model for testing the pulmonary toxicity of complex mixtures such as cigarette smoke. Experimental and Toxicologic Pathology, 55 (1), 51–57. [PubMed: 12940629]

Avila A, et al. , 2000. An electrochemical approach to investigate gated electron transfer using a physiological model system: cytochrome c immobilized on carboxylic acid-terminated alkanethiol self-assembled monolayers on gold electrodes. The Journal of Physical Chemistry B, 104 (12), 2759–2766.

Banan Sadeghian R, et al. , 2017. Macroporous mesh of nanoporous gold in electrochemical monitoring of superoxide release from skeletal muscle cells. Biosensors & Bioelectronics, 88, 41–47. [PubMed: 27474045]

Bérubé K, et al. , 2009. In vitro models of inhalation toxicity and disease. Alta, 37, 89–141.

Blank F, et al. , 2006. An optimized in vitro model of the respiratory tract wall to study particle cell interactions. Journal of Aerosol Medicine, 19 (3), 392–405. [PubMed: 17034314]

Bowden EF, Hawkridge FM, and Blount HN, 1984. Interfacial electrochemistry of cytochrome c at tin oxide, indium oxide, gold, and platinum electrodes. Journal of Electroanalytical Chemistry, 161 (2), 355–376.

Cai CX, Ju HX, and Chen HY, 1995. The effects of temperature and electrolyte on the redox potential of cytochrome c at a chemically modified microband gold electrode. Electrochimica Acta, 40 (9), 1109–1112.

Calas-Blanchard C, Catanante G, and Noguer T, 2014. Electrochemical sensor and biosensor strategies for ROS/RNS detection in biological systems. Electroanalysis, 26 (6), 1277–1286.

Carrasco-Torres G, et al. , 2017. Cytotoxicity, oxidative stress, cell cycle arrest, and mitochondrial apoptosis after combined treatment of hepatocarcinoma cells with maleic anhydride derivatives and quercetin. Oxidative Medicine and Cellular Longevity, 2017, 2734976. [PubMed: 29163752]

Carter WO, Narayanan PK, and Robinson JP, 1994. Intracellular hydrogen peroxide and superoxide anion detection in endothelial cells. Journal of Leukocyte Biology, 55 (2), 253–258. [PubMed: 8301222]

Chen W, et al. , 2012. Recent advances in electrochemical sensing for hydrogen peroxide: a review. The Analyst, 137 (1), 49–58. [PubMed: 22081036]

Chen XJ, et al. , 2008. Detection of the superoxide radical anion using various alkanethiol monolayers and immobilized cytochrome c. Analytical Chemistry, 80 (24), 9622–9629. [PubMed: 19072268]

Chiu J and Dawes IW, 2012. Redox control of cell proliferation. Trends in Cell Biology, 22 (11), 592–601. [PubMed: 22951073]

Cho WS, et al. , 2012. Differential pro-inflammatory effects of metal oxide nanoparticles and their soluble ions in vitro and in vivo; zinc and copper nanoparticles, but not their ions, recruit eosinophils to the lungs. Nanotoxicology, 6 (1), 22–35. [PubMed: 21332300]

Davies KJ, 1999. The broad spectrum of responses to oxidants in proliferating cells: a new paradigm for oxidative stress. IUBMB Life, 48 (1), 41–47. [PubMed: 10791914]

de Bruijne K, et al. , 2009. Design and testing of electrostatic aerosol in vitro exposure system (EAVES): an alternative exposure system for particles. Inhalation Toxicology, 21 (2), 91–101. [PubMed: 18800273]

Eguílaz M, Gutiérrez A, and Rivas G, 2016. Non-covalent functionalization of multi-walled carbon nanotubes with cytochrome c: enhanced direct electron transfer and analytical applications. Sensors and Actuators B: Chemical, 225, 74–80.

Elihn K, et al. , 2013. Cellular dose of partly soluble cu particle aerosols at the air-liquid interface using an in vitro lung cell exposure system. Journal of Aerosol Medicine and Pulmonary Drug Delivery, 26 (2), 84–93. [PubMed: 22889118]

Finkel T, 2003. Oxidant signals and oxidative stress. Current Opinion in Cell Biology, 15 (2), 247–254. [PubMed: 12648682]

Fisher AB, 2009. Redox signaling across cell membranes. Antioxidants & Redox Signaling, 11 (6), 1349–1356. [PubMed: 19061438]

Frijns E, et al. , 2017. A novel exposure system termed NAVETTA for in vitro laminar flow electrodeposition of nanoaerosol and evaluation of immune effects in human lung reporter cells. Environmental Science & Technology, 51 (9), 5259–5269. [PubMed: 28339192]

Fröhlich E, et al. , 2013. Comparison of two in vitro systems to assess cellular effects of nanoparticles-containing aerosols. Toxicology In Vitro, 27 (1), 409–417. [PubMed: 22906573]

Ganesana M, Erlichman JS, and Andreescu S, 2012. Real-time monitoring of superoxide accumulation and antioxidant activity in a brain slice model using an electrochemical cytochrome c biosensor. Free Radical Biology & Medicine, 53 (12), 2240–2249. [PubMed: 23085519]

Gerhardt N, Clothier R, and Wild G, 2014. Investigating the practicality of hazardous material detection using unmanned aerial systems. 2014 IEEE international workshop on metrology for aerospace. 2014 – proceedings, 133–137.

Gomez-Mingot MG, et al. , 2014. Screen-printed graphite macroelectrodes for the direct electron transfer of cytochrome c: a deeper study of the effect of pH on the conformational states, immobilization and peroxidase activity. The Analyst, 139 (6), 1442–1448. [PubMed: 24492631]

Gopal D, et al. , 1988. Cytochrome c: ion binding and redox properties. The Journal of Biological Chemistry, 263 (24), 11652–11656. [PubMed: 2841331]

Gosens I, et al. , 2016. Organ burden and pulmonary toxicity of nanosized copper (II) oxide particles after short-term inhalation exposure. Nanotoxicology, 10 (8), 1084–1095. [PubMed: 27132941]

Haber VF and Weiss J, 1932. Uber die katalyse des hydroperoxydes. Die Naturwissenschaften, 20 (51), 948–950.

Halliwell B and Whiteman M, 2004. Measuring reactive species and oxidative damage in vivo and in cell culture: how should you do it and what do the results mean? British Journal of Pharmacology, 142 (2), 231–255. [PubMed: 15155533]

Izyumskaya N, et al. , 2017. Review—electrochemical biosensors based on ZnO nanostructures. ECS Journal of Solid State Science and Technology, 6 (8), Q84–Q100.

Jing X, et al. , 2015. Toxicity of copper oxide nanoparticles in lung epithelial cells exposed at the air-liquid interface compared with in vivo assessment. Toxicology In Vitro, 29 (3), 502–511. [PubMed: 25575782]

Kalyanaraman B, et al. , 2012. Measuring reactive oxygen and nitrogen species with fluorescent probes: challenges and limitations. Free Radical Biology & Medicine, 52 (1), 1–6. [PubMed: 22027063]

Kim JS, et al. , 2011. Effects of copper nanoparticle exposure on host defense in a murine pulmonary infection model. Particle and Fibre Toxicology, 8, 29–14. [PubMed: 21943386]

Kim JS, et al. , 2013. Validation of an in vitro exposure system for toxicity assessment of air-delivered nanomaterials. Toxicology In Vitro, 27 (1), 164–173. [PubMed: 22981796]

Lai X, et al. , 2018. Intranasal delivery of copper oxide nanoparticles induces pulmonary toxicity and fibrosis in C57BL/6 mice. Scientific Reports, 8, 1–12. [PubMed: 29311619]

LeBel CP, Ischiropoulos H, and Bondy SC, 1992. Evaluation of the probe 2′,7′-dichlorofluorescin as an indicator of reactive oxygen species formation and oxidative stress. Chemical Research in Toxicology, 5 (2), 227–231. [PubMed: 1322737]

Lenz AG, et al. , 2009. A dose-controlled system for air–liquid interface cell exposure and application to zinc oxide nanoparticles. Particle and Fibre Toxicology, 6 (1), 32. [PubMed: 20015351]

Lewinski NA, Secondo LE, and Ferri JK, 2018. Enabling real-time hazard assessment at the workplace enabling real-time hazard assessment at the workplace. 14th global Congress on process safety. Orlando: American Institute of Chemical Engineers, 1–9.

Li X, et al. , 2010. Real-time electrochemical monitoring of cellular H_2O_2 integrated with in situ selective cultivation of living cells based on dual functional protein microarrays at Au-TiO_2 surfaces. Analytical Chemistry, 82 (15), 6512–6518. [PubMed: 20583800]

Lieber M, et al. , 1976. A continuous tumor-cell line from a human lung carcinoma with properties of type II alveolar epithelial cells. International Journal of Cancer, 17 (1), 62–70. [PubMed: 175022]

Liu X, et al. , 2016. Real-time investigation of antibiotics-induced oxidative stress and superoxide release in bacteria using an electrochemical biosensor. Free Radical Biology & Medicine, 91, 25–33. [PubMed: 26655038]

Luo Y, et al. , 2009. Detection of extracellular H_2O_2 released from human liver cancer cells based on TiO_2 nanoneedles with enhanced electron transfer of cytochrome c. Analytical Chemistry, 81 (8), 3035–3041. [PubMed: 19290667]

Matson U, Ekberg LE, and Afshari A, 2004. Measurement of ultrafine particles: a comparison of two handheld condensation particle counters. Aerosol Science and Technology, 38 (5), 487–495.

Mills JB, Hong Park J, and Peters TM, 2013. Comparison of the DiSCmini aerosol monitor to a handheld condensation particle counter and a scanning mobility particle sizer for submicrometer sodium chloride and metal aerosols. Journal of Occupational and Environmental Hygiene, 10 (5), 250–258. [PubMed: 23473056]

Murphy MP, 2009. How mitochondria produce reactive oxygen species. The Biochemical Journal, 417 (1), 1–13. [PubMed: 19061483]

Myhre O, et al. , 2003. Commentary evaluation of the probes 2′,7′-dichlorofluorescin diacetate, luminol, and lucigenin as indicators of reactive species formation. Biochemical Pharmacology, 65 (10), 1575–1582. [PubMed: 12754093]

Oberdörster G, et al. , 2005. Principles for characterizing the potential human health effects from exposure to nanomaterials: elements of a screening strategy. Particle and Fibre Toxicology, 2, 8. [PubMed: 16209704]

Park E-J, et al. , 2008. Oxidative stress induced by cerium oxide nanoparticles in cultured BEAS-2B cells. Toxicology, 245 (1–2), 90–100. [PubMed: 18243471]

Pettibone JM, et al. , 2008. Inflammatory response of mice following inhalation exposure to iron and copper nanoparticles. Nanotoxicology, 2 (4), 189–204.

Prieto-Simón B, et al. , 2008. Electrochemical biosensors as a tool for antioxidant capacity assessment. Sensors and Actuators B: Chemical, 129 (1), 459–466.

Rahimi P, Ghourchian H, and Rafiee-Pour H-A, 2011. Superoxide radical biosensor based on a nano-composite containing cytochrome c. The Analyst, 136 (18), 3803–3808. [PubMed: 21804961]

Rani VS, et al. , 2013. Pulmonary toxicity of copper oxide (CuO) nanoparticles in rats. Journal of Medical Sciences (Faisalabad), 13 (7), 571–577.

Rodkey FL and Ball EG, 1950. Oxidation-reduction potentials of the cytochrome c system. Journal of Biological Chemistry, 182, 17–28.

Rui Q, et al. , 2010. Electrochemical biosensor for the detection of H_2O_2 from living cancer cells based on ZnO nanosheets. Analytica Chimica Acta, 670 (1–2), 57–62. [PubMed: 20685417]

Sadeghian RB, et al. , 2016. Online monitoring of superoxide anions released from skeletal muscle cells using an electrochemical biosensor based on thick-film nanoporous gold. ACS Sensors, 1 (7), 921–928.

Santschi C, et al. , 2017. Non-invasive continuous monitoring of pro-oxidant effects of engineered nanoparticles on aquatic microorganisms. Journal of Nanobiotechnology, 15, 1–18. [PubMed: 28049488]

Savolainen K, et al., 2013. Nanosafety in Europe 2015–2025: towards safe and sustainable nanomaterials and nanotechnology innovations. Finnish Institute of Occupational Health.

Scognamiglio V, 2013. Nanotechnology in glucose monitoring: advances and challenges in the last 10 years. Biosensors & Bioelectronics, 47, 12–25. [PubMed: 23542065]

Secondo LE, Wygal NJ, and Lewinski NA, 2019. A new Portable In Vitro Exposure Cassette for aerosol sampling. Journal of Visualized Experiments, 144, 1–11.

Šimšíková M and Antalík M, 2013. Interaction of cytochrome c with zinc oxide nanoparticles. Colloids and Surfaces. B, Biointerfaces, 103, 630–634. [PubMed: 23274157]

Tammeveski K, et al. , 1998. Superoxide electrode based on covalently immobilized cytochrome c: modelling studies. Free Radical Biology and Medicine, 25 (8), 973–978. [PubMed: 9840743]

Thirumalai D, et al. , 2017. Electrochemical reactive oxygen species detection by cytochrome c immobilized with vertically aligned and electrochemically reduced graphene oxide on a glassy carbon electrode. The Analyst, 142 (23), 4544–4552. [PubMed: 29114650]

Tiwari AJ, Fields CG, and Marr LC, 2013. A cost-effective method of aerosolizing dry powdered nanoparticles. Aerosol Science and Technology, 47 (11), 1267–1275.

Vietti G, Lison D, and Van Den Brule S, 2016. Mechanisms of lung fibrosis induced by carbon nanotubes: towards an adverse outcome pathway (AOP). Particle and Fibre Toxicology, 13, 11–23. [PubMed: 26926090]

Vilcekova S, Burdova EK, and Snopkova M, 2013. Environmental assessment of selected building – case study. GeoConference on nano, bio and green – technologies for a sustainable future, 633–647.

Wittekindt OH, et al., 2014. In vitro toxicology systems. New York, NY: Humana Press.

Zhou J, et al. , 2014. Molecular hydrogel-stabilized enzyme with facilitated electron transfer for determination of H_2O_2 released from live cells. Analytical Chemistry, 86 (9), 4395–4401. [PubMed: 24716876]

Zhu A, et al. , 2009. Nanoporous gold film encapsulating cytochrome c for the fabrication of a H_2O_2 biosensor. Biomaterials, 30 (18), 3183–3188. [PubMed: 19264356]

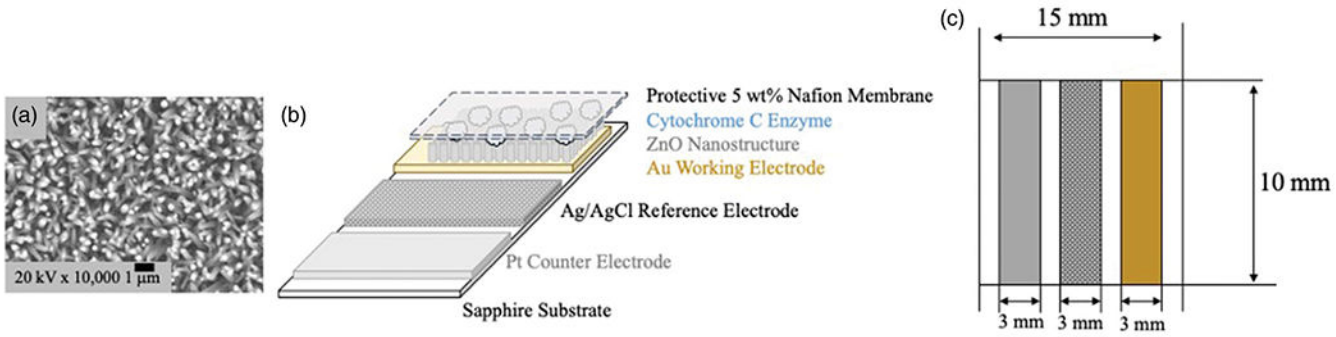

Figure 1.

Design of coplanar tri-electrode sensor. (a) SEM image of ZnO nanorods. (b) Schematic of sensor design. (c) Top view of sensor design.

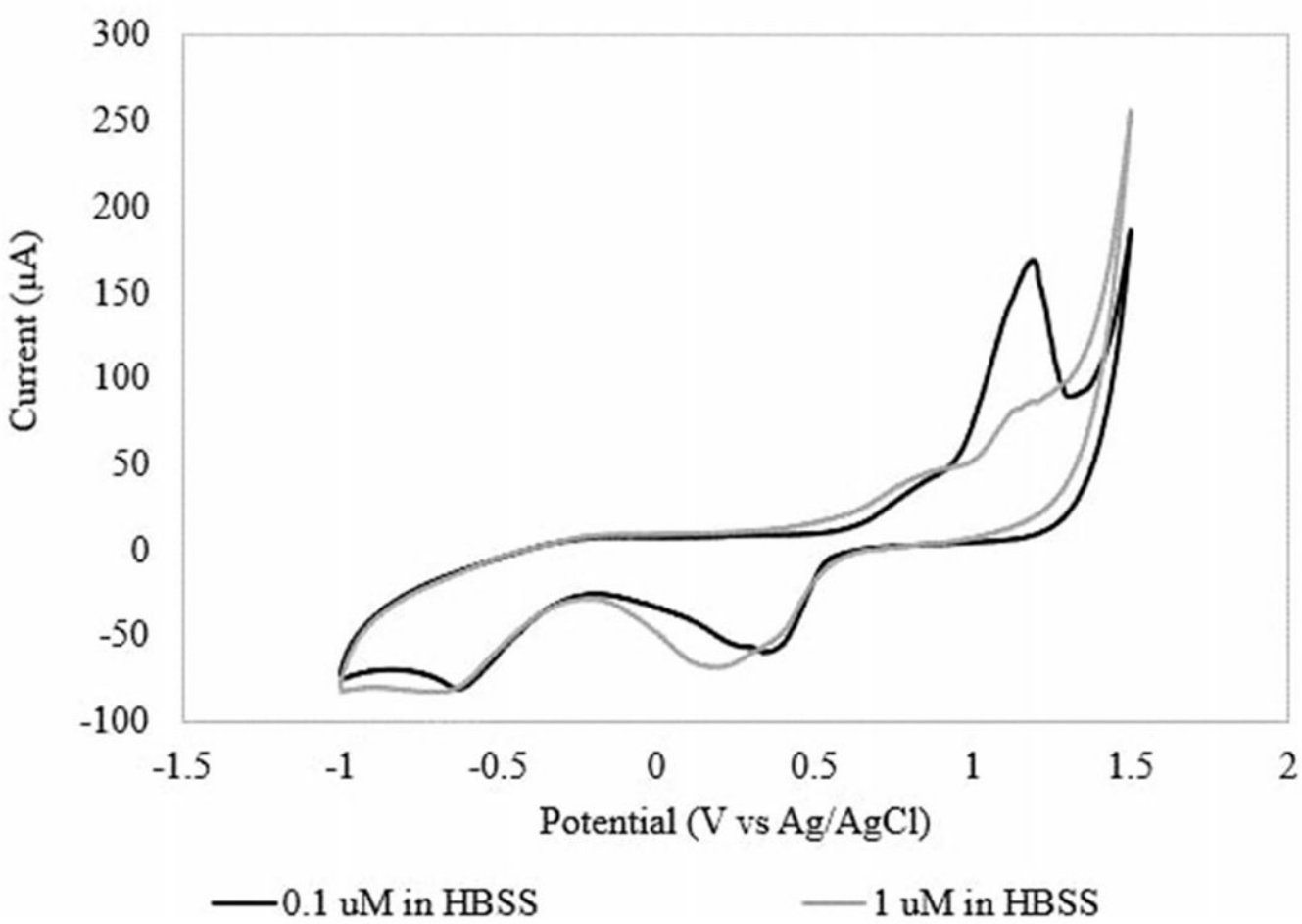

Figure 2.
CV curves of 0.1 µM H_2O_2 in HBSS and 1 µM H_2O_2 in HBSS.

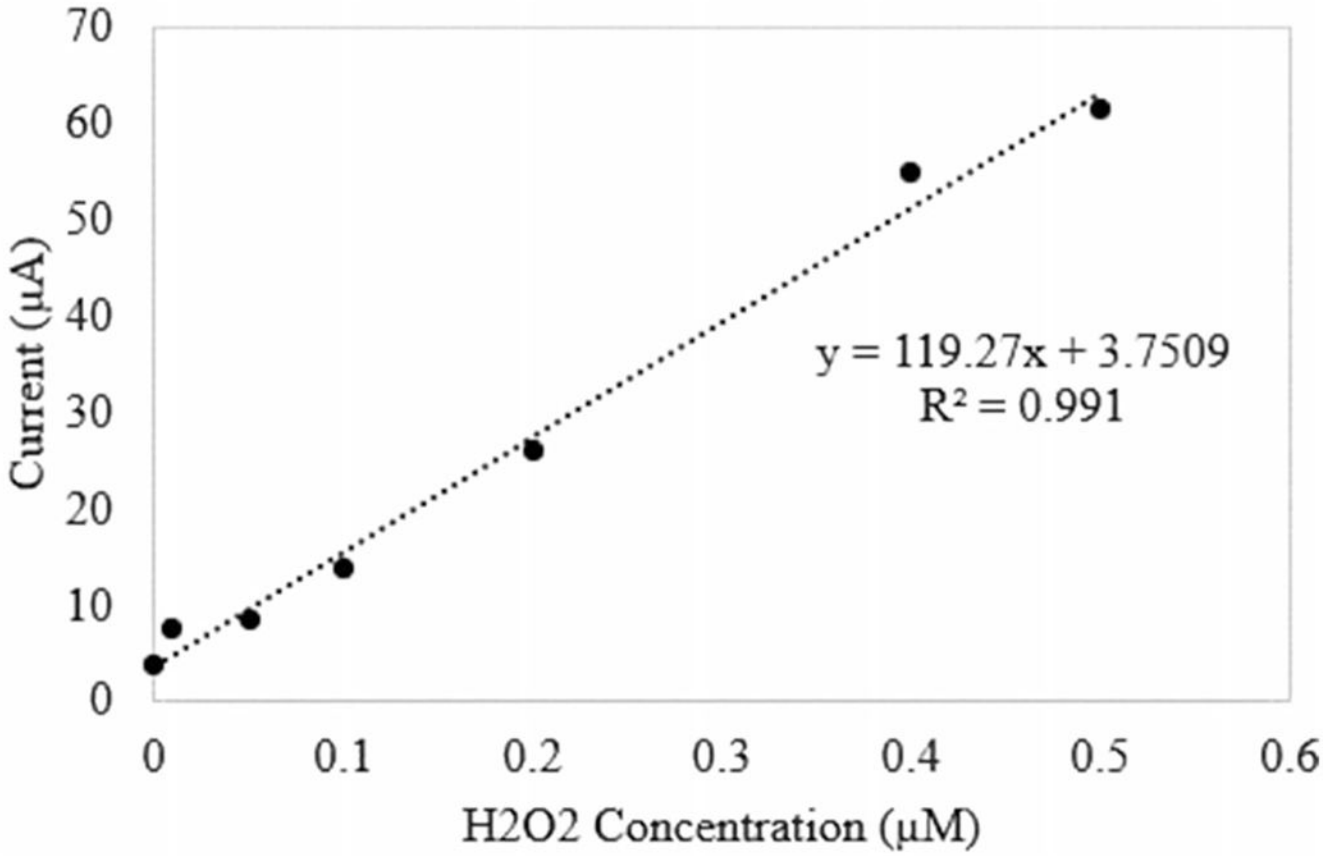

Figure 3.
Calibration curve for ROS sensor at 1 V versus Ag/AgCl.

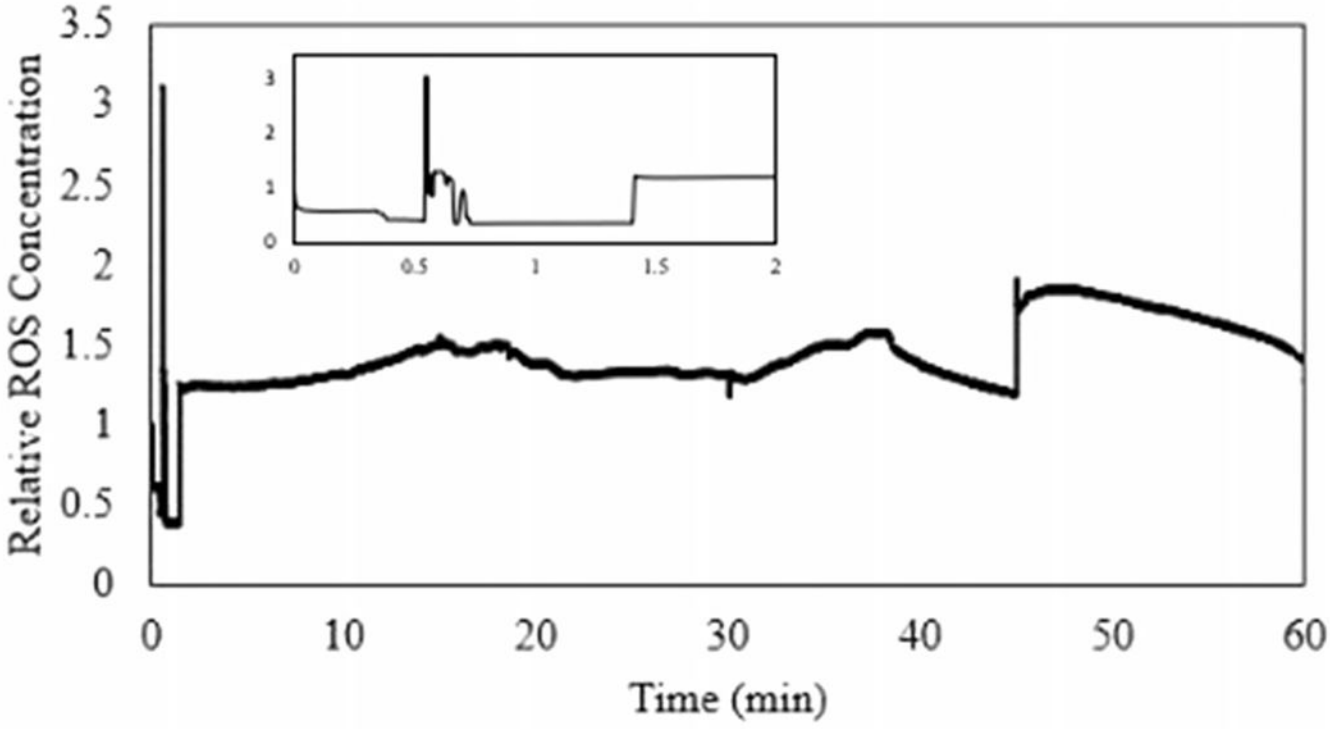

Figure 4.
Extracellular ROS generation measured by sensor.

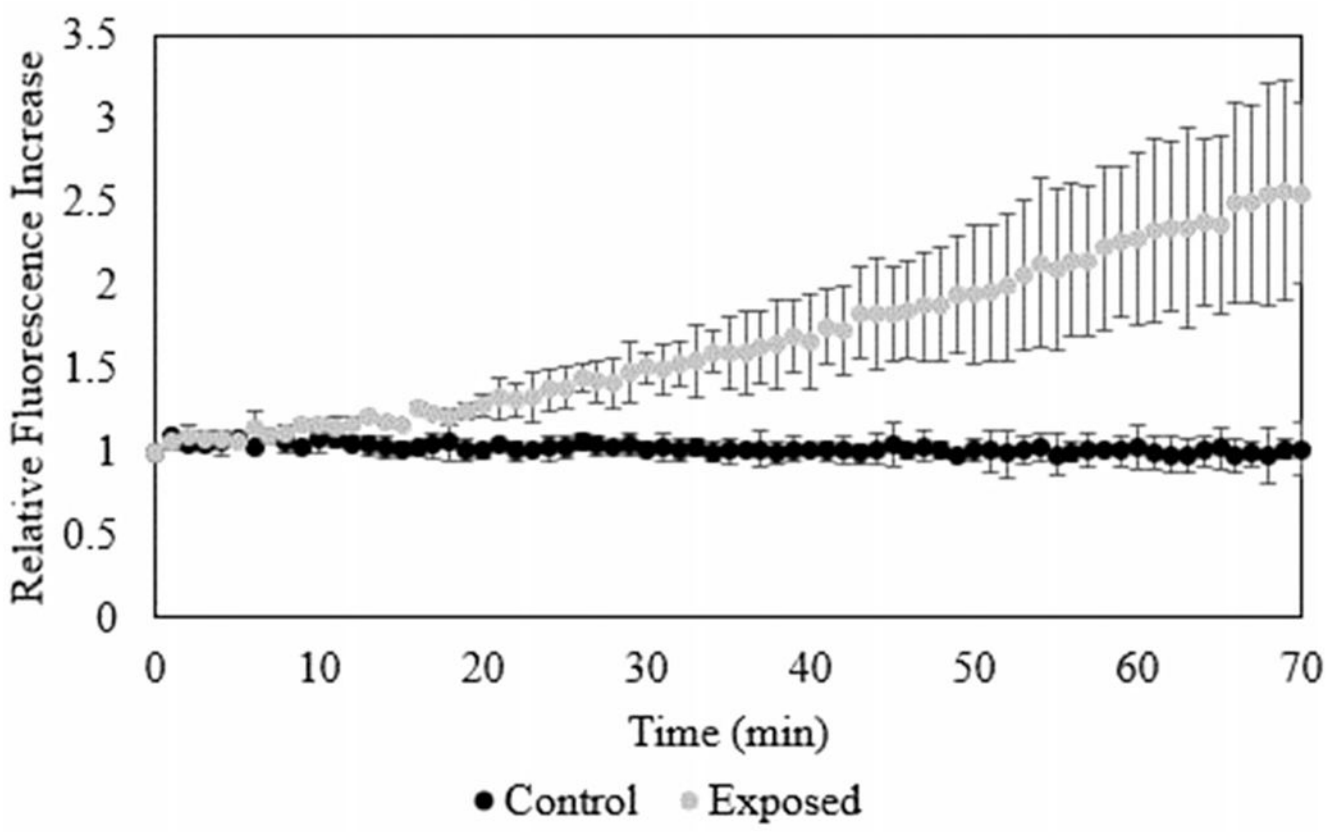

Figure 5.
Intracellular ROS generation measured by the DCFH-DA assay.